IEEE Access
Multidisciplinary | Rapid Review | Open Access Journal

Received June 17, 2020, accepted June 30, 2020, date of publication July 3, 2020, date of current version July 15, 2020.

Digital Object Identifier 10.1109/ACCESS.2020.3006894

Fault Detection of WECSs With a Delayed Input and an Unknown Part Based on SVO

RUINAN ZHAO AND YANXIA SHEN
Engineering Research Center of IoT Technology and Application of the Ministry of Education, Jiangnan University, Wuxi 214122, China
Corresponding author: Yanxia Shen (shenyx@jiangnan.edu.cn)

This work was supported in part by the National Nature Science Foundations under Grant 61573167 and Grant 61572237, in part by the Fundamental Research Funds for the Central Universities under Grant JUSRP31106 and Grant JUSRP51510, and in part by the Postgraduate Research and Practice Innovation Program of Jiangsu Province under Grant KYCX17_1459.

ABSTRACT This paper studies an improved set-valued observer (SVO) for a complex model of a wind energy conversion system (WECS). To fit reality, an unknown function is used to describe the aerodynamic model, and a delay of the input signal is added to simulate the actual situation. The conservative SVO estimates the state error convergence within an adjustable interval. The extended Lipschitz condition, set-induced theory, and uniformly ultimately boundedness guarantees the convergence of errors. Based on the SVO, a fault detection system and corresponding fault detection strategies for common faults of WECSs are proposed. By adjusting the gain matrix L, the SVO shows excellent state tracking performance. The simulation results show that the proposed fault detection system can provide rapid and accurate fault detection.

INDEX TERMS Extended Lipschitz condition, fault detection strategies, SVO, set-induced theory, uniformly ultimately boundedness, unknown function, WECS.

I. INTRODUCTION

As more countries continue to increase the installed capacity of wind power, the research and development, control of wind energy conversion system (WECS) have become a hotspot of research. Generally, wind farms are mostly located over offshore waters, on islands, on plateaus, and in other inhospitable places with good wind energy reserves. A WECS has a complex structure, in an unfavorable physical environment, frequent faults occur. The application of efficient fault detection technology could reduce operation costs. Therefore, research on the fault detection of WECSs has practical significance. At present, the research objectives of WECSs are mainly focused on single components, such as a blade pitch [1], [2], doubly fed induction generator [3], [4], or permanent magnet synchronous generator [5]. The research targets of fault detection are mainly focused on a variety of models, such as a permanent magnet synchronous motor drives [6], polytopic linear parameter-varying system [7], heterogeneous multiagent LPV system [8], linear discrete time-varying system [9], and T-S fuzzy system with local nonlinear models [10]. The above studies have similar disadvantages, for example, in the study of linear mathematical models and their derived subsystem models, the existence of communication delays was not considered, and nonlinear models were rarely established. Therefore, it was of significant value to establish a complex model of a WECS with an unknown nonlinear part and communication delays and research the fault detection problem based on an observer with simple structure and good state tracking capability.

For a nonlinear or an uncertain system, in recent years, the algorithms of state estimation were mostly concentrated on complex state observer or intelligence algorithms. Abid *et al.* [11] established an RBFNNs-based observer, residual generation, and fault detectability condition. Simulation results of a DC motor showed the good state tracking of the observer and the good fault detection ability of the fault detection schemes. Guo *et al.* [12] used T-S fuzzy models to approximate a discrete nonlinear system and designed a variable gain observer. The simulation results showed that the sensor and actuator fault detection for the time-varying gain observer was very close to that of the constant gain observer. Fezai *et al.* [13] researched variable moving window kernel principal component analysis (VMWKPCA) for a continuous stirred tank reactor. The simulation results presented that the fault diagnosis using different partial VMWKPCAs detected the fault correctly and quickly. Shahnazari and Mhaskar [14] offered a high gain observer in the presence of uncertainty.

The associate editor coordinating the review of this manuscript and approving it for publication was Francesco Tedesco.

The simulation results showed that the residuals obtained from the given fault detection and isolation mechanism had high precision. For output-constrained switched MIMO nonstrict-feedback nonlinear systems with an unknown dead zone, Ma *et al.* [15] approximated the uncertain nonlinearities with neural networks and the unavailable states with a switched MIMO observer. The simulation results showed good state tracking trajectories of the designed observer-based adaptive control. For the fault detection of uncertain systems with quantization, Xiong *et al.* [16] established a residual generation method based on a quantized signal and designed a robust nonfragile fault detection filter. The RNFDFQ detected the fault effectively. For uncertain switched nonlinear systems, Zhao *et al.* [17] studied a fuzzy-approximation-based asymptotic tracking control method to track the controlled states. The simulation results showed that this algorithm had fewer oscillations than the algorithm developed by Zhao *et al.* [18]. The above algorithms were complex, and it was of great significance to study an observer with both a simple structure and a good state tracking performance.

For the state observations, set-valued theory provides an adjustable interval estimation solution called set-valued observer (SVO). Lin *et al.* [19] proposed an algorithm based on a uniformly bounded theory and multivertex estimation, which were the foundations of the SVO adopted in this paper. Rosa *et al.* [20] proposed a complete theory for a fault detection and isolation (FDI) scheme based on another form of SVO. Further, Rosa established several FDI filters with similar structures. For a single sensor [21], Rosa established two parallel SVOs to ensure the logical correctness of the FDI. As an extended study, a type of FDI filter containing four parallel SVOs and one parallel nominal FD filter [22] was established. Further, a global SVO [23] was added to replace the nominal FD filter to guarantee the performance of fault detection. The simulation results provided by Rosa verified that the SVO had a good state tracking performance, and that the fault detection strategies based on SVO could accurately detect the common faults. Therefore, it is of great significance to improve the SVO and apply it to the fault detection of complex WECSs.

In this paper, the fault detection of a faulted WECS with a delayed input and an unknown part based on SVO was studied. An improved SVO was researched to track the status and detect faults. After confirming the Lipschitz property of the unknown part, the application of uniformly bounded set and set-induced Lyapunov function guaranteed the boundedness and convergence of the observer. By adjusting the gain matrix, the SVO could exhibit excellent state tracking performance. Based on the SVO, fault detection strategies were proposed for some common faults that occur in WECSs.

The structure of this paper is as follows. In Section 2, the mathematical model of WECS with a delayed input and an unknown part is given. In Section 3, an improved SVO is designed. In Section 4, the fault detection system and corresponding fault detection strategies are provided. In Section 5, the numerical simulation for four faults and fault detections and comparative study are discussed. Finally, Section 6 presents the conclusion.

II. MODEL OF A WECS WITH A DELAYED INPUT AND AN UNKNOWN PART

A WECS contains several subsystems, including the wind model, pitch system, aerodynamics, tower shadow, drive train, generator, and converter [24]. Considering the interaction effect of the subsystems [25], the relationships of the subsystems are listed in Figure 1.

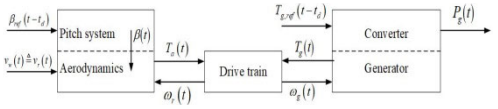

FIGURE 1. Relationships of the subsystems.

The time-delay factor t_d represents the communication delay to the pitch actuator and the converter, which depends on the communication distance, communication line, and communication equipment. For a single wind power tower, the influences of the above three conditions on the communication delays of the pitch actuator and converter can be considered equal. Therefore, this paper assumes that the communication delays of the pitch actuator and converter are equal. For each subsystem, the mathematical models are presented as follow:

1). The pitch system is modeled as a second-order system with a time delay, described as

$$\ddot{\beta}(t) = -2\zeta\omega_n\dot{\beta}(t) - \omega_n^2\beta(t) + \omega_n^2\beta_{ref}(t - t_d).$$

where $\beta(t)$ is the pitch angle [°], $\beta_{ref}(t - t_d)$ is the delayed reference input of $\beta(t)$ [°], and t_d is the value of the delay time to the system [s]. This is a generic description of a single pitch for a general three-pitch WECS. There are slight differences among the pitch angles due to the different phases between the three pitches. In this paper, it is assumed that the three pitches have the same angle, described by the above formula.

2). The aerodynamics are modeled via an unknown nonlinear system, described as

$$T_a(t) = \rho\pi R^2 v_r^3(t) C_p(\lambda(t), \beta(t)) \Big/ 2\omega_r(t).$$

where $T_a(t)$ is the aerodynamic torque [Nm], $\omega_r(t)$ is the rotor speed [rad/s], $v_r(t)$ is the rotor effective wind speed [m/s], and $C_p(\lambda(t), \beta(t))$ is the power coefficient. $\lambda(t)$ is the tip-speed ratio. The free wind speed $v_w(t)$ includes the mean wind speed, tower shadow, turbulence, and wind shear component [26]. The free wind acting on the pitches causes tower displacement. Then, the rotor effective wind speed $v_r(t)$ can be obtained. This process is complex [27]. To simplify the model, this paper assumes that the tower has no displacement, omits the calculation processes of the tower shadow, turbulence, and wind shear, and uses the free wind speed $v_w(t)$ to replace the rotor effective wind speed $v_r(t)$.

$C_p(\lambda(t), \beta(t))$ is an unknown function with $\lambda(t)$ and $\beta(t)$ as variables. The surface diagram of $C_p(\lambda(t), \beta(t))$ is presented in Figure 2 as follows

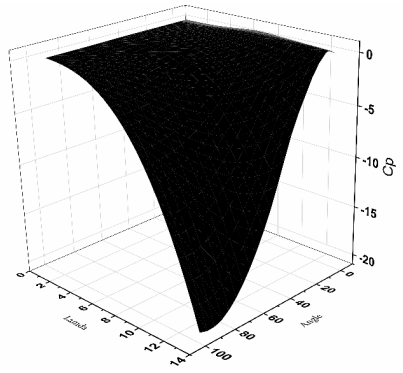

FIGURE 2. The 3D figure of the power coefficient $C_p(\lambda(t), \beta(t))$.

3). The drive train is modeled as three first-order differential equations, described as

$$\dot{\omega}_r(t) = \frac{T_a(t)}{J_r} - \frac{K_{dt}\theta_\Delta(t)}{J_r} - \frac{(B_{dt}+B_r)}{J_r}\omega_r(t) + \frac{B_{dt}}{N_g J_r}\omega_g(t),$$
$$\dot{\omega}_g(t) = \frac{K_{dt}}{N_g J_g}\theta_\Delta(t) + \frac{B_{dt}}{N_g J_g}\omega_r(t) - \left(\frac{B_{dt}}{N_g^2 J_g} + \frac{B_g}{J_g}\right)\omega_g(t) - \frac{T_g(t)}{J_g},$$
$$\dot{\theta}_\Delta(t) = \omega_r(t) - \frac{1}{N_g}\omega_g(t).$$

where $\theta_\Delta(t)$ is the torsion angle of the drive train [rad/s], $\omega_g(t)$ is the generator speed [rad/s], and $T_g(t)$ is the generator torque [Nm].

4). The converter is modeled as a first-order system with a time delay, described as

$$\dot{T}_g(t) = -\frac{1}{\tau_g}T_g(t) + \frac{1}{\tau_g}T_{g,ref}(t - t_d).$$

where $T_{g,ref}(t - t_d)$ is the delayed reference input to the generator torque [Nm].

Thus, the model of the WECS with a delayed input and an unknown nonlinear part is assembled from the above subsystems. The description of the model is presented as follows

$$\begin{aligned} \dot{X}(t) &= AX(t) + BU(t) + B_d U_d(t - t_d) + \Phi(t, X, U), \\ Y &= CX(t), \\ X_s(t) &= X(t) + ED(t). \end{aligned} \tag{1}$$

where

$$X(t) = \left[\omega_r(t) \quad \omega_g(t) \quad \theta_\Delta(t) \quad T_g(t) \quad \beta(t) \quad \dot{\beta}(t)\right]^T,$$
$$U(t) = v_{r,m}(t),$$
$$U_d(t - t_d) = \left[T_{g,ref}(t - t_d) \quad \beta_{ref}(t - t_d)\right]^T,$$
$$A = \begin{bmatrix} -\frac{(B_{dt}+B_r)}{J_r} & \frac{B_{dt}}{N_g J_r} & \frac{K_{dt}}{J_r} & 0 & 0 & 0 \\ \frac{B_{dt}}{N_g J_g} & -\left(\frac{B_{dt}}{N_g^2 J_g} + \frac{B_g}{J_g}\right) & \frac{K_{dt}}{N_g J_g} & -\frac{1}{J_g} & 0 & 0 \\ 1 & -\frac{1}{N_g} & 0 & 0 & 0 & 0 \\ 0 & 0 & 0 & -\frac{1}{\tau_g} & 0 & 0 \\ 0 & 0 & 0 & 0 & 0 & 1 \\ 0 & 0 & 0 & 0 & -\omega_n^2 & -2\zeta\omega_n \end{bmatrix},$$
$$B = \left[0 \quad 0 \quad 0 \quad 0 \quad 0 \quad 0\right]^T,$$
$$B_d = \begin{bmatrix} 0 & 0 & 0 & 0 & 0 & \omega_n^2 \\ 0 & 0 & 0 & \frac{1}{\tau_g} & 0 & 0 \end{bmatrix}^T,$$
$$\Phi(t, X, U) = \begin{bmatrix} \frac{1}{J_r} & 0 & 0 & 0 & 0 & 0 \end{bmatrix}^T \times T_a(t, X, U).$$

$X_s(t)$ is the vector of the measured values of the state vector $X(t)$. $v_{r,m}(t) = v_w(t) + d(t)$ represents the measured value of the rotor effective wind speed $v_r(t)$. $ED(t)$ is a white noise that affects all the sensors.

III. IMPROVED SVO DESIGN

A. DESIGN OF IMPROVED SVO

In this section, for system (1), an improved SVO is designed to estimate the states in an adjustable interval. The form of the improved SVO is presented as follows

$$\dot{\hat{X}}(t) = (A - LC)\hat{X}(t) + BU(t) + B_d U_d(t - t_d) + \hat{\Phi}\left(t, \hat{X}, U\right) + LY. \tag{2}$$

Thus, the estimation error $e(t) = \hat{X}(t) - X(t)$ is expressed as follows

$$\dot{e}(t) = (A - LC)e(t) + Ln(t) + \left(\hat{\Phi}\left(t, \hat{X}, U\right) - \Phi(t, X, U)\right). \tag{3}$$

where $n(t)$ is a corresponding matrix used to reduce the range of L, which is determined by the ranges of the states.

To prove that the estimation error (3) converges to a given interval, some theoretical expressions are given below. First, the Euler approximating system is used to discretize the continuous system as follows

$$x(k + 1) = \left(I + \varepsilon A_g\right)x(k) + \varepsilon B_g u(k). \tag{4}$$

where A_g and B_g represent the parameters of a general linear continuous system. Generally, $\varepsilon = 1$. This system can be

applied only if the sampling time k is small enough. By applying equation (4) to the estimation error (3), the discrete system can be obtained as follows

$$e(k+1) = [I + (A - LC)]\, e(k) + Ln(k) + \left(\hat{\Phi}\left(k, \hat{X}, U\right) - \Phi(k, X, U)\right). \quad (5)$$

Equation (5) is divided into two parts: The nonlinear part

$$Ped_1 = \hat{\Phi}\left(k, \hat{X}, U\right) - \Phi(k, X, U). \quad (6)$$

and the main part

$$Ped_2 = [I + (A - LC)]\, e(k) + Ln(k). \quad (7)$$

A similar formula partitioning can be applied to systems (1) and (2) to obtain the corresponding nonlinear parts and main parts.

Definition 1 [11]: There exists a matrix M that satisfied

$$g(a) - g(b) \leq M(a - b). \quad (8)$$

where a and b belong to the domain of $g(x)$, which is called the extended Lipschitz condition of the nonlinear function $g(x)$.

Corollary 1: Taking the upper and lower limits of the domain of $g(x)$, namely, x_u and x_d, the inequality (8) is simplified to

$$g(a) - g(b) \leq M(a - b) \leq M(x_u - x_d). \quad (9)$$

Definition 2 [28], [29]: A C-set is a convex and compact set containing the origin states within it, which can be represented by the symbol *int* {}.

Definition 3 [28], [29]: If there exists a set $\Theta_0 \subset \Theta$, for every initial condition $x(0) \in \Theta_0$, and every output $y \in Y$ and $t \geq 0$, it can be assumed that the system $x(k+1) = Ax(k) + Ed(k)$ is **uniformly bounded** in the C-set Θ and $x \in \Theta$. The C-set Θ can be regarded as a **positive** D-invariant for the system. Further, adding a condition $x(t) \in int\{\Theta\}$, the system $x(k+1) = Ax(k) + Ed(k)$ is said to be **uniformly ultimately bounded** in the C-set Θ. The C-set Θ can be regarded as a **strong positive** D-invariant for the system.

Definition 4 [28], [29]: For a given constant μ constrained within the closed interval [0, 1], and any $x \in \Theta$, if there exist $\dot{X} = \{\dot{x} : \dot{x}(t) = Ax(t) + Ed(t); \forall d \in D\} \subset \mu\Theta$, then the set Θ is μ-contractive.

The set Θ that satisfies **Definition 2-4** can be rewritten as a linear matrix inequality $\Theta = \{x : Fx \leq \Sigma\}$. The matrix F stands for the corresponding matrix. The symbol *vert* {}, which stands for the set of vertices of the polytope, and Z_j, which stands for the corresponding convex cone for a specific vertex v_j of Θ are illustrated in Figure 3 as follows

$$Z_j = \left\{f_i^T x \leq \varsigma_i, \varsigma_i > 0, \quad for\ every\ f_i\ and\ \varsigma_i\right\}$$
$$f_i^T v_j = \varsigma_i, \quad for\ every\ v_j \in vert\{\Theta\}.$$

The characteristic of a strong positive D-invariant is transitive. It is confirmed that Θ is a strong positive D-invariant region for the continuous-time system, if the region Θ is a strong positive D-invariant region for its matched Euler approximating system. Thus, the following proposition can be derived for system (5):

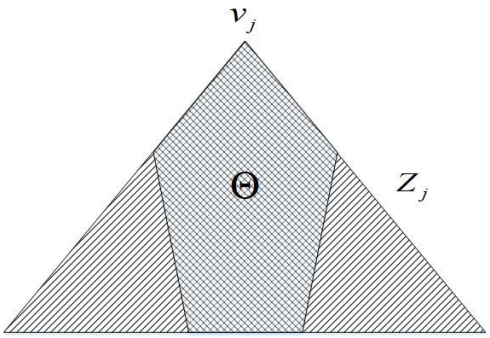

FIGURE 3. The relationship of convex cone Z_j and region Θ.

Proposition 1: The region Θ is a strong positive D-invariant for system (5); if and only if there exist a constant μ that satisfied $0 < \mu < 1$, for every vertex $v_j \in vert\{\Theta\}$ and every vertex $d_h \in vert\{D\}$, there exists

$$v_j + (A - LC)\, v_j + Ln(k) + \left(\hat{\Phi}\left(k, \hat{X}, U\right) - \Phi(k, X, U)\right) \in \mu\varsigma_j + M_n(X_u - X_d). \quad (10)$$

where $M_n(X_u - X_d)$ is the corresponding region of nonlinear part (6). Hence, inequality (12) can be derived as follows

$$v_j + (A - LC)\, v_j + Ln(k) + Ped_1 \in \mu Z_j + M_n(X_u - X_d). \quad (11)$$

Therefore, the range of the gain matrix L can be calculated from the set of linear inequalities as follows:

$$f_i^T v_j + f_i^T (A - LC)\, v_j + f_i^T Ln(k) < \mu\varsigma_i + M_n(X_u - X_d). \quad (12)$$

Since the range of L is affected by v_j and $n(t)$, and not every matrix in the range can meet the requirement, the explicit value of L can be determined by performing several simulations.

B. CONVERGENCE OF THE ESTIMATION ERROR

Before providing the proof of the convergence of the estimation error, a gauge function is introduced as follows

A gauge function $\Psi : R^n \to R$ satisfies the following conditions:

1) $\Psi(a + b) \leq \Psi(a) + \Psi(b)$;
2) $\Psi(x)$ is nonnegative;
3) $\Psi(a) = 0 \Leftrightarrow a = 0$;
4) for $\sigma > 0$, $\Psi(\sigma a) = \sigma\Psi(a)$.

This function defines a linear distance between the original state $x(0)$ and $x(t)$ in every possible direction. The ball B_r of radius r in reference to Ψ is defined as $B_r = \{x : \Psi(x) \leq r\}$. Based on the Minkowski function $\Psi_\Theta(e) = max\left\{f_i^T e\right\}$, a C-set P is regarded as the unit ball $\Psi_P(x)$ as follows

$$\Psi_P(x) = \begin{cases} 0 & x = 0 \\ 1, & where\ x \in \partial(P)\ \ otherwise \end{cases}$$

Since $\partial(P)$ has to be extended to contain x, so there exist $x \in P \Leftrightarrow \Psi_P \leq 1$.

According to the gauge function and **Definition 2-4**, two more lemmas are obtained as follows:

Lemma 1: If region Θ is a strong positive D-invariant set for the main part of system (1) with convergence rate $\mu \leq 1$, then $\vartheta\Theta$ has the same property for all $\vartheta \geq 1$.

Lemma 2: If and only if there exists a gauge function $\Psi(e)$ satisfying the condition that the unit ball $B_1 \subset \Theta$, a region Θ is a strong positive D-invariant set for the main part of system (1) with the convergence rate $\mu < 1$. If $e \notin int\{B_1 + B_{Mn}\}$, where B_{Mn} is the corresponding function of the item $M_n(X_u - X_d)$, then B_ϑ is μ-contractive for all $\vartheta \geq 1$.

According to the lemmas above, the boundedness of estimation error (3) can be derived as follows:

Define set Θe as a C-set that corresponds to the item $Z_j + M_n(X_u - X_d)$. Define $\Psi_{\Theta e}(e)$ as a Minkowski function. For all $e(k)$ satisfying $e(k) \in R^n$ and $e(k) \notin int\{\Theta e\}$, there exist $\Psi_{\Theta e}(e(k+1)) \leq \lambda\Psi_{\Theta e}(e(k))$ according to inequality (13) and **Lemma 2**. Generated from the set Θe for all accurate μ, $\Psi_{\Theta e}(e)$ is a function that defines stability. This function has been identified as a set-induced stability function. The convergence of the estimation error to Θe is implied by the set-induced stability function according to **Lemma 2**. By utilizing the Euler approximating system, the convergence is certain for $\Psi_{\Theta e}(e(k+1)) \leq \lambda\Psi_{\Theta e}(e(k))$. For any original condition of the estimation error $e(t_0)$, there exists $e(t) \in \Theta e$ and $X(t) + e(t) \in \hat{X}(t)$, where time t is large enough.

IV. FAULT DETECTION SYSTEM AND FAULT DETECTION STRATEGIES

In this paper, a fault detection system based on one global SVO is provided. The structure of the fault detection system is provided in the following Figure 4.

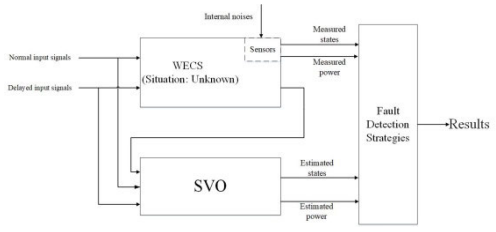

FIGURE 4. The structure of the fault detection system.

The principles of fault detection:

Error evaluation is an important basis for fault detection, which is described by the error evaluation function $J(e(t))$ and the threshold value J_{th}, where $e(t)$ represents the estimation error of the state that requires fault detection. Thus, the fault can be detected based on the following assumptions:

$$J(e(t)) > J_{th} \Rightarrow faulted$$
$$J(e(t)) \leq J_{th} \Rightarrow fault - free.$$

In this paper, a universal error evaluation function is adopted, as follows:

$$J(e) = \frac{|e|}{S_{norm}} \times 100\%.$$

where S_{norm} represents the normal value of the corresponded state. If there exists a rated value S_{rated} for a state, then $S_{norm} = S_{rated}$. For the three-pitch WECS pitch angle $\beta_i(t)$ wherer $i = 1, 2, 3$, $S_{norm} = \beta_j(t)$ where $j = 1, 2, 3$ and $j \neq i$. Therefore, for actuator faults and sensor faults, this paper designs corresponding fault detection strategies as follows:

Fault detection strategy of actuator faults:

Step 1: Two thresholds are set: a normal operation threshold $J_{th1} = 5\%$ and a maximum range threshold $J_{th2} = 10\%$.

Step 2: The error evaluation function $J(e(t))$ is calculated for the following data: the normal value of the state and the estimated value of SVO, marked as first priority data $J(e(t))_1$; the normal value of the output power and the estimated value of output power calculated from the states of SVO, marked as second priority data $J(e(t))_2$.

Step 3: If $J(e(t))_1 \leq J_{th1}$, the system is judged to be fault-free. Continue to **Step 5**; If $J_{th1} < J(e(t))_1 \leq J_{th2}$, the system is judged to be faulted. Continue to **Step 4**; For a state with a rated value, if $J(e(t))_1 > J_{th2}$, the system is judged to have a high-hazard fault, which needs emergency treatment. Continue to **Step 5**; For a state without a rated value, if $J(e(t))_1 > J_{th2}$, but the estimated values of SVO are still within the allowable range, then turn to **Step 4**; Otherwise, the system is judged to have a high-hazard fault, which needs emergency treatment. Continue to **Step 5**.

Step 4: If $J(e(t))_2 \leq J_{th2}$, the system is judged to have a low-hazard fault, which is fault-tolerant; If $J(e(t))_2 > J_{th2}$, the system is judged to have a high-hazard fault, which needs emergency treatment.

Step 5: End.

Fault detection strategy for sensor faults:

Step 1: One threshold is set: a normal operation threshold $J_{th3} = 5\%$.

Step 2: The error evaluation function $J(e(t))$ is calculated for the following data: the estimated value of the SVO and the sensor output value, marked as $J(e(t))_3$.

Step 3: If $J(e(t))_3 \leq J_{th3}$, the sensor is judged to be fault-free; If $J(e(t))_3 > J_{th3}$, the sensor is judged to be faulted, which needed to be addressed. Continue to **Step 4.**

Step 4: End.

V. SIMULATION STUDIES

This paper chooses a 4.8 MW WECS benchmark model as the simulation object. The parameters are listed in the following Table 1.

TABLE 1. Values of the WECS properties.

Symbol	Quantity	Value
B_r	Viscous friction coefficient of the low speed shaft	7.11 Nm(rad/s)
B_g	Viscous friction coefficient of the high speed shaft	45.6 Nm(rad/s)
J_r	Moment of inertia of the low speed shaft	5.5×10^7 kgm^2
J_g	Moment of inertia of the high speed shaft	390 kgm^2
B_{dt}	Torsional damping coefficient of the drive train	775.49 Nm(rad/s)
K_{dt}	Torsional stiffness of the drive train	2.7×10^9 Nm/rad
N_g	Ratio of the drive train	95
τ_g	Time constant of the first-order system	0.02
ω_n	Pitch actuator model natural frequency	11.11 rad/s
ξ	Pitch actuator model damping ratio	0.6
ρ	Air density	1.225 kg/m^3
R	Radius of the cross section of the pitch sweep	57.5 m

Therefore, the coefficient matrices are as follows

$$A=\begin{bmatrix} -1.4229\times10^{-5} & 1.4842\times10^{-7} & -49.0909 \\ 0.0209 & -0.1171 & 7.2874\times10^{4} \\ 1 & -0.0105 & 0 \\ 0 & 0 & 0 \\ 0 & 0 & 0 \\ 0 & 0 & 0 \end{bmatrix}$$

$$\begin{bmatrix} 0 & 0 & 0 \\ -0.0026 & 0 & 0 \\ 0 & 0 & 0 \\ -50 & 0 & 0 \\ 0 & 0 & 1 \\ 0 & -123.4321 & -13.3320 \end{bmatrix},$$

$$B_d=\begin{bmatrix} 0 & 0 & 0 & 50 & 0 & 0 \\ 0 & 0 & 0 & 0 & 0 & 123.4321 \end{bmatrix}^T,$$

$$C=\begin{bmatrix} 0 & 1 & 0 & 0 & 0 & 0 \\ 0 & 0 & 0 & 1 & 0 & 0 \end{bmatrix},$$

$$E=\begin{bmatrix} 1 & 1 & 1 & 1 & 1 & 1 \end{bmatrix}.$$

By choosing different vertexes v_j, corresponding matrices f_i^T and $\mu = 0.9$, the range of each element of the matrix L can be obtained as

$$L=\begin{bmatrix} 20 & 14360 & -0.6 & 1 & -0.6 & -2.6 \\ 243 & 8400 & 0.3 & -40 & 0.3 & -110 \end{bmatrix}.$$

In the rest of this section, simulations of the normal system and fault detection results of 4 specific fault cases classified by Sloth [24] are presented.

Case I: No faults:

From Figures 5-6, it is obvious that the order of magnitude of the estimation error is extremely low, which means the state tracking performance of the SVO is excellent.

Case II: Sensor fault of generator speed ω_g

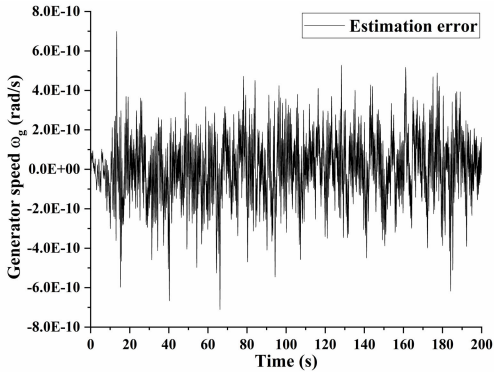

FIGURE 5. The estimation error of the generator speed ω_g between the normal value and the estimated value of the SVO.

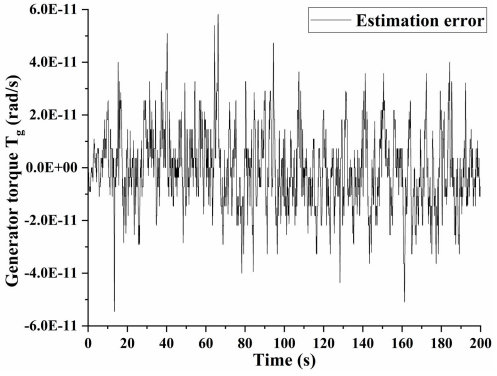

FIGURE 6. The estimation error of the generator torque T_g between the normal value and the estimated value of the SVO.

In this section, the sensor fault of the generator speed ω_g is simulated. For a sensor, the typical faults can be classified into two types: no output and fixed output. The two types of sensor faults are identical in the mathematical model. Assuming that a fixed output fault of generator speed ω_g occurred at $t_s = 130.0s$ and ended at $t_e = 140.0s$, the simulation results are presented in the following Figures 7-8.

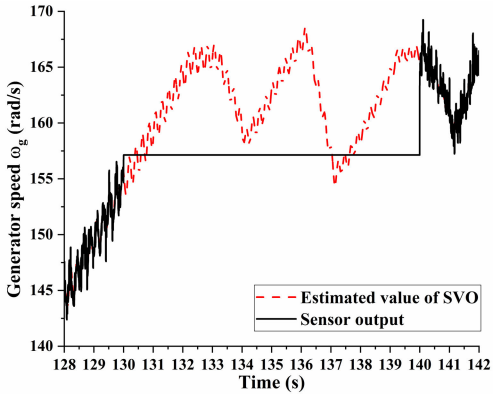

FIGURE 7. Simulation result of the generator speed ω_g under fault Case II.

From Figure 7-8, the fixed output fault of a single state can be detected accurately by the given fault detection strategy.

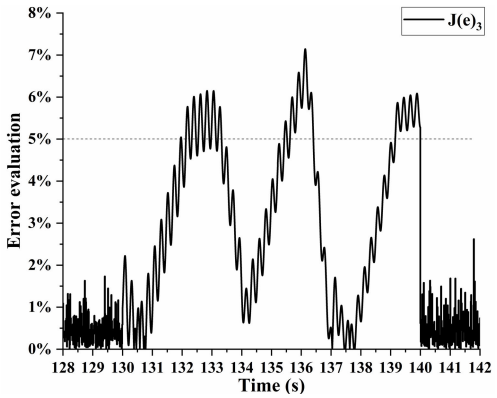

FIGURE 8. Trajectory of error evaluation $J\,(e)_3$ under fault Case II.

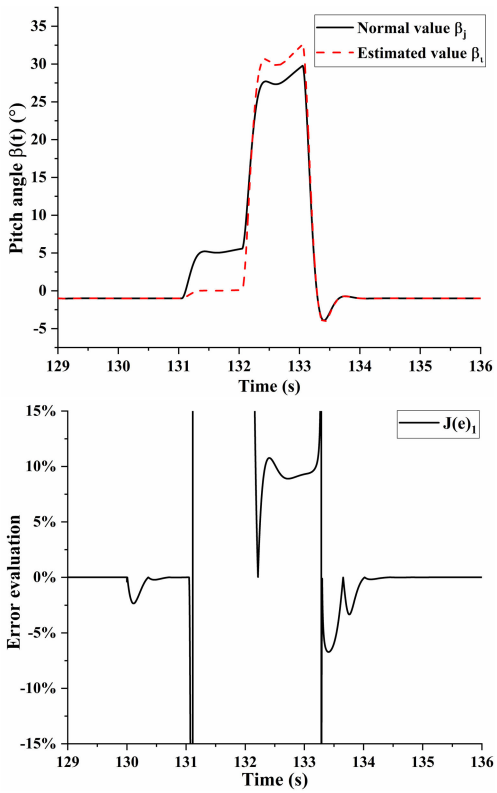

FIGURE 9. Simulation result and error evaluation of pitch angle β under fault Case III where $i = 1, 2, 3, j = 1, 2, 3$ and $j \neq i$.

From Figure 8, it is obvious that the selection of the threshold J_{th3} directly affects the response time and accuracy of fault detection. For $J_{th3} = 5\%$, the occurrence of fault **Case II** is determined to be at $t_{fd} = 132.13s$. If reducing the threshold to $J_{th3} = 2\%$, the response time of fault detection will be drastically reduced, but a fault misjudgment point is observed near $t = 142s$. If the sensor output is lost, it is believed that the fault detection process of this fault is similar to that of fault **Case II.**

Case III: Hydraulic leak of pitch system

Assuming that the hydraulic cylinder of the hydraulic pitch leaks at $t_s = 130.0s$, and returns to normal at $t_e = 140.0s$, the mathematical model of this fault is described as the parameter changes in the state equation of the pitch angle $\beta\,(t)$. Sloth [24] proposed a simplified parameters variation equations as follows

$$\tilde{\zeta}\,(t) = (1 - \alpha_{hlm}\,(t))\,\zeta + \alpha_{hlm}\,(t)\,\zeta_{hl}\,(t)$$
$$\tilde{\omega}_n\,(t) = (1 - \alpha_{hlm}\,(t))\,\omega_n + \alpha_{hlm}\,(t)\,\omega_{n,hl}\,(t)$$

where $\xi_{hl} = 0.9$ and $\omega_{n,hl} = 3.42rad/s$. Suppose that ζ and ω_n change linearly from $t_s = 130.0s$ to $t_{md} = 135.0s$, namely, α_{hlm} linearly increases from 0 to 1 in $5s$, but remains constant from $t_{md} = 135.0s$ to $t_e = 140.0s$. The simulation results are presented in the following Figures 9-10.

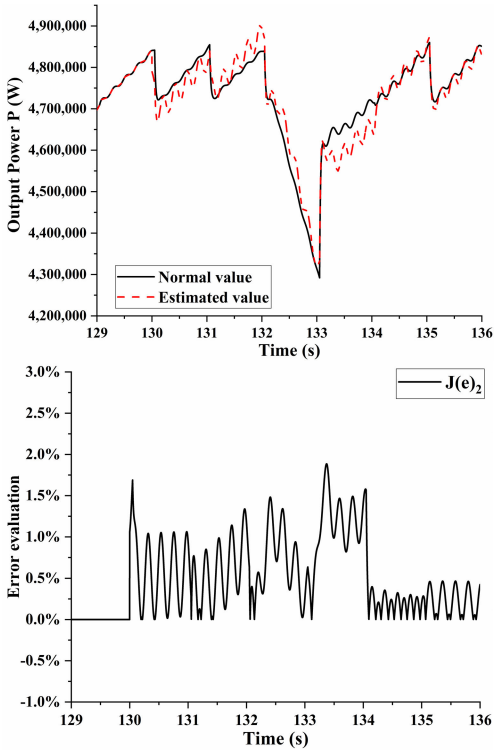

FIGURE 10. Simulation result and error evaluation of output power P under fault Case III.

From Figures 9-10, it is clear that fault **Case III** can be detected correctly. Although fault **Case III** causes considerable fluctuations (the evaluation of estimation error is much larger than the threshold J_{th2}), the pitch angle still fluctuates within the allowable range $(0 - 90°)$. In addition, the power fluctuation is acceptable (the corresponded error evaluation is lower than the threshold J_{th2}). Therefore, the low-hazard in fault **Case III** can be judged at $t_{fd} = 131.06s$, and the system can operate in fault-tolerant operation for a short time. Notably, $\hat{\beta}_i\,(t)$ reaches the critical point $(90°)$ at $t_{st} = 139.79s$ and then exhibits a sharp upward trend. At this point, the pitch is out of control, and the system needs to be stopped for maintenance.

Case IV: Valve block or pump block of the pitch system

The mathematical models of a valve block and pump block can be viewed as the same model. Assuming the valve or

pump of the pitch system blocks at $t_s = 101.5s$ and returns to normal at $t_e = 111.5s$, the corresponding state is fixed during a certain time. In this case, the fixed pitch angle $\beta_{fix} = 21.7517°$. The simulation results are listed in the following Figures 11-12.

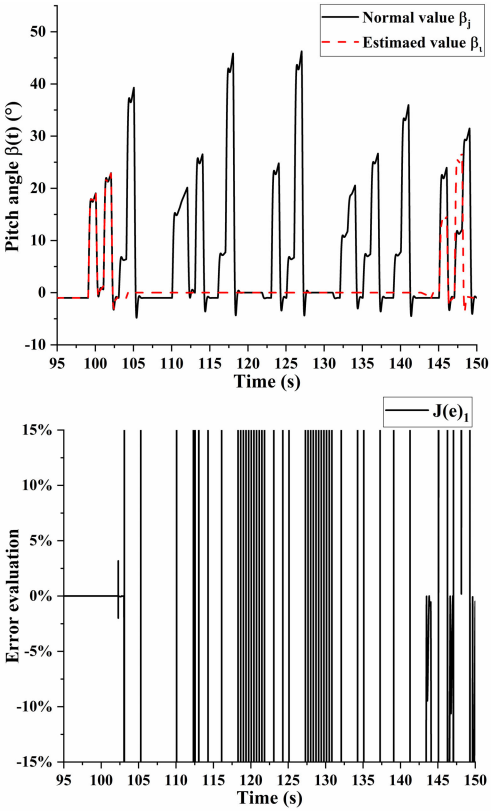

FIGURE 11. Simulation result and error evaluation of the pitch angle β under fault Case IV.

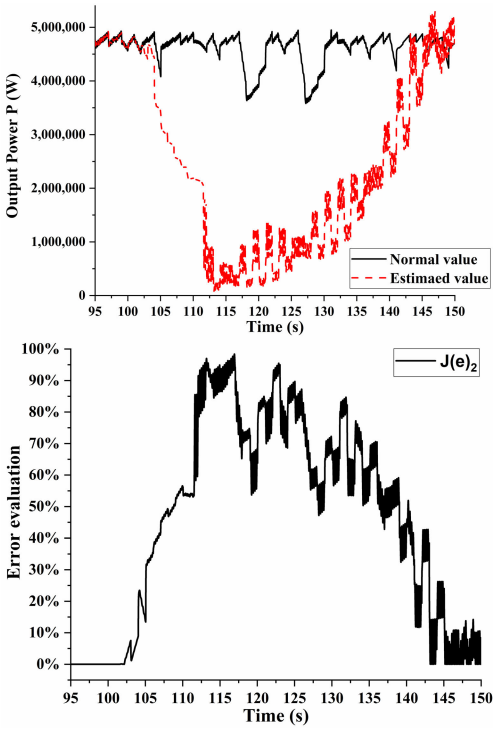

FIGURE 12. Simulation result and error evaluation of the output power P under fault Case IV.

TABLE 2. FDT of five strategies.

FD strategy	Simulation object	FDT (s)
RBFNNs	WECS under **fault case III**	1.55
VGO		1.84(threshold = 0.5)
VMWKPCA		1.50(threshold = 0.5)
HGO		3.02
SVO		1.06

From Figures 11-12 it is clear that fault **Case IV** can be detected correctly. Although fault **Case IV** causes considerable fluctuations (the evaluation of estimation error is much larger than the threshold J_{th2}), the pitch angle still fluctuates within the allowable range $(0 - 90°)$. However, at $t_{fd} = 104.06$, the error evaluation is $J(e)_2 > J_{th2}$, and it is judged that the high-hazard fault **Case IV** occurred.

Case V: Offset

Assuming the offset of the generator torque occurred at $t_s = 130.0s$ instantly, the SVO is very sensitive to the fault of the generator torque. For fault **Case V**, the estimated generator torque $\hat{T}_g$ tends toward negative infinity at $t_{ter} = 130.92s$, and the SVO terminates the operation. Therefore, fault **Case V** can be detected and located successfully.

Defining the fault detection time (FDT) as $t_{\text{det}} = t_{fd} - t_s$, it is considered an important index to evaluate the performance of fault detection strategy. In the following Table 2, the comparison between the proposed strategy and RBFNNs [11], variable gain observer (VGO) [12], VMWKPCA [13], and high-gain observer (HGO) [14] for determining fault detection time are given. It is clear that the FDT of the SVO and FD strategy is less than that of the four other FD strategies.

VI. CONCLUSION

In this paper, a mathematical WECS with a delayed input and an unknown nonlinear part has been established, and an improved SVO for the nonlinear system has been designed. On this basis, fault detection strategies based on a single global SVO have been designed. The improved SVO for a linear model with a delayed input and an unknown nonlinear part has inherited the high-precision state tracking capability, controllable conservatism, and simple structure of the basic SVO. As a kind of conservative state observer, the extended Lipschitz condition constrains the range of the unknown part, and the set-induced theory and uniformly ultimately boundedness guarantee the stability of the improved SVO. Regarding common faults of a WECS, this paper has offered fault detection strategies for actuator faults and sensor faults based on one single global SVO. For the four fault cases, the simulation results show that the fault detection strategies locate the faults accurately and quickly. The comparative

study of the FDT presents that the proposed SVO and FD strategy has the fastest response to the fault. In the future, the control of WECS with a delayed input and an unknown part will be considered.

REFERENCES

[1] M. A. Ebrahim, H. S. Ramadan, and M. Soliman, "Robust non-fragile approach to resilient design of PID-based blade pitch control for wind energy conversion system," *Asian J. Control*, vol. 21, no. 4, pp. 1952–1965, Jul. 2019.

[2] B. E. Elnaghi, M. E.-S. Dessouki, and F. A. Elkader, "Experimental investigation of pitch angle controller for DFIG based wind energy conversion system," in *Proc. 19th Int. Middle East Power Syst. Conf. (MEPCON)*, Cairo, Egypt, Dec. 2017, pp. 1477–1482.

[3] Z. Tir, O. P. Malik, and M. N. Hashemnia, "Intelligent control of a brushless doubly-fed induction generator," *Int. J. Syst. Assurance Eng. Manage.*, vol. 10, no. 3, pp. 326–338, Jun. 2019.

[4] N. E. Karakasis and C. A. Mademlis, "High efficiency control strategy in a wind energy conversion system with doubly fed induction generator," *Renew. Energy*, vol. 125, pp. 974–984, Sep. 2018.

[5] A. Omar, F. Khater, and A. Shaltout, "Per unit modeling of wind energy conversion system based on PMSG," in *Proc. Int. Conf. Adv. Control Circuits Syst. (ACCS), Int. Conf. New Paradigms Electron. Inf. Technol. (PEIT)*, Alexandria, Egypt, 2018, pp. 117–126.

[6] M. Bourogaoui, H. B. A. Sethom, and I. S. Belkhodja, "Real-time encoder faults detection and rotor position estimation for permanent magnet synchronous motor drives fault tolerant sensorless control using digital signal controller," *Math. Comput. Simul.*, vol. 131, pp. 253–267, Jan. 2017.

[7] M. Zhou, M. Rodrigues, Y. Shen, and D. Theilliol, "$H\_/H_\infty$ fault detection observer design based on generalized output for polytopic LPV system," *J. Phys., Conf. Ser.*, vol. 783, Jan. 2017, Art. no. 012002.

[8] M. Chadli, M. Davoodi, and N. Meskin, "Distributed fault detection and isolation filter design for heterogeneous multi-agent LPV systems," in *Proc. Amer. Control Conf. (ACC)*, Seattle, WA, USA, May 2017, pp. 1610–1615.

[9] Y. Li, H. R. Karimi, Q. Zhang, D. Zhao, and Y. Li, "Fault detection for linear discrete time-varying systems subject to random sensor delay: A Riccati equation approach," *IEEE Trans. Circuits Syst. I, Reg. Papers*, vol. 65, no. 5, pp. 1707–1716, May 2018.

[10] D. Zhai, A.-Y. Lu, J. Dong, and Q.-L. Zhang, "Event triggered $H\_/H_\infty$ fault detection and isolation for T-S fuzzy systems with local nonlinear models," *Signal Process.*, vol. 138, pp. 244–255, Sep. 2017.

[11] W. Abid, A. Krifa, and N. Liouane, "Neural observer-based small fault detection and isolation for uncertain nonlinear systems," *Int. J. Adapt. Control Signal Process.*, vol. 34, no. 5, pp. 677–702, Feb. 2020.

[12] S. Guo, F. Zhu, W. Zhang, S. H. Żak, and J. Zhang, "Fault detection and reconstruction for discrete nonlinear systems via Takagi-Sugeno fuzzy models," *Int. J. Control, Autom. Syst.*, vol. 16, no. 6, pp. 2676–2687, Dec. 2018.

[13] R. Fezai, M. Mansouri, O. Taouali, M. F. Harkat, and N. Bouguila, "Fault diagnosis for dynamic nonlinear system based on variable moving window KPCA," in *Proc. 15th Int. Multi-Conf. Syst., Signals Devices (SSD)*, Hammamet, Tunisia, Mar. 2018, pp. 590–595.

[14] H. Shahnazari and P. Mhaskar, "Simultaneous actuator and sensor fault isolation of nonlinear systems subject to uncertainty," in *Proc. Amer. Control Conf. (ACC)*, Boston, MA, USA, Jul. 2016, pp. 6857–6862.

[15] L. Ma, X. Huo, X. Zhao, and G. D. Zong, "Observer-based adaptive neural tracking control for output-constrained switched MIMO nonstrict-feedback nonlinear systems with unknown dead zone," *Nonlinear Dyn.*, vol. 99, no. 2, pp. 1019–1036, Jan. 2020.

[16] J. Xiong, X.-H. Chang, and X. Yi, "Design of robust nonfragile fault detection filter for uncertain dynamic systems with quantization," *Appl. Math. Comput.*, vol. 338, pp. 774–788, Dec. 2018.

[17] X. Zhao, X. Wang, L. Ma, and G. Zong, "Fuzzy approximation based asymptotic tracking control for a class of uncertain switched nonlinear systems," *IEEE Trans. Fuzzy Syst.*, vol. 28, no. 4, pp. 632–644, Apr. 2020.

[18] X. Zhao, X. Zheng, B. Niu, and L. Liu, "Adaptive tracking control for a class of uncertain switched nonlinear systems," *Automatica*, vol. 52, pp. 185–191, Feb. 2015.

[19] H. Lin, G. Zhai, and P. J. Antsaklis, "Set-valued observer design for a class of uncertain linear systems with persistent disturbance," in *Proc. Amer. Control Conf.*, Denver, CO, USA, 2003, pp. 1902–1907.

[20] P. Rosa, P. Casau, C. Silvestre, S. M. Tabatabaeipour, and J. Stoustrup, "A set-valued approach to FDI and FTC: Theory and implementation issues," *IFAC Proc. Volumes*, vol. 45, no. 20, pp. 1281–1286, Jan. 2012.

[21] P. Rosa, C. Silvestre, J. S. Shamma, and M. Athans, "Fault detection and isolation of LTV systems using set-valued observers," in *Proc. 49th IEEE Conf. Decis. Control (CDC)*, Atlanta, GA, USA, Dec. 2010, pp. 768–773.

[22] P. Rosa and C. Silvestre, "Fault detection and isolation of LPV systems using set-valued observers: An application to a fixed-wing aircraft," *Control Eng. Pract.*, vol. 21, no. 3, pp. 242–252, Mar. 2013.

[23] P. Rosa, C. Silvestre, J. S. Shamma, and M. Athans, "Fault detection and isolation of an aircraft using set-valued observers," *IFAC Proc. Volumes*, vol. 43, no. 15, pp. 398–403, 2010.

[24] C. Sloth, T. Esbensen, and J. Stoustrup, "Robust and fault-tolerant linear parameter-varying control of wind turbines," *Mechatronics*, vol. 21, no. 4, pp. 645–659, Jun. 2011.

[25] H. Habibi, H. R. Nohooji, and I. Howard, "Power maximization of variable-speed variable-pitch wind turbines using passive adaptive neural fault tolerant control," *Frontiers Mech. Eng.*, vol. 12, no. 3, pp. 377–388, Sep. 2017.

[26] H. Habibi, I. Howard, and S. Simani, "Reliability improvement of wind turbine power generation using model-based fault detection and fault tolerant control: A review," *Renew. Energy*, vol. 135, pp. 877–896, May 2019.

[27] P. F. Odgaard, J. Stoustrup, and M. Kinnaert, "Fault-tolerant control of wind turbines: A benchmark model," *IEEE Trans. Control Syst. Technol.*, vol. 21, no. 4, pp. 1168–1182, Jul. 2013.

[28] F. Blanchini, "Feedback control for linear time-invariant systems with state and control bounds in the presence of disturbances," *IEEE Trans. Autom. Control*, vol. 35, no. 11, pp. 1231–1234, Nov. 1990.

[29] H. Lin, G. Zhai, and P. J. Antsaklis, "Set-valued observer design for a class of uncertain linear systems with persistent disturbance and measurement noise," *Int. J. Control*, vol. 76, no. 16, pp. 1644–1653, Nov. 2003.